Simulation study on the classification efficiency of hydrocyclone with double vortex finders

Estudio de simulación sobre la eficiencia en la clasificación por hidrociclones con boquillas de doble vortex

Yuekan Zhang[1], Peikun Liu[1], Junru Yang[1], Xinghua Yang[1] and Yuying Yan[2]

[1] College of Mechanical and Electronic Engineering, Shandong University of Science and Technology, Qianwangang Road 579#, Qingdao, 266590, Shandong, China
[2] Faculty of Engineering, the university of Nottingham. University Park, Nottingham, NG7 2RD, United Kingdom

DOI: http://dx.doi.org/10.6036/8050 | Recibido: 09/03/2016 • Aceptado: 07/07/2016

RESUMEN

- La clasificación de eficiencia de los hidrociclones es uno de los problemas fundamentales que requieren soluciones que promuevan el desarrollo de un sistema de separación sólido-líquido. Se propone un nuevo modelo de hidrociclón para mejorar la estructura tradicional y la precisión en la clasificación de eficiencia. Por lo tanto, un tubo de rebosadura coaxial con un diámetro pequeño se inserta en el tubo original, lo que hace posible obtener tres diferentes productos con diferentes grados de tamaño en un ciclo. Posteriormente, usando la dinámica de fluidos computacional, el modelo de estrés de Reynolds se introdujo en el Reynolds-promediado de Navier-Stokes; el modelo matemático de mezcla sólido-líquido de flujo multifásico fue establecido. Finalmente, un estudio sobre la simulación de los efectos de los parámetros estructurales (por ejemplo, sub-desbordamiento diámetro de orificio, el diámetro interno del tubo de rebose, e insertó la profundidad del tubo de desbordamiento interno) sobre la clasificación de eficiencia de subdesbordamiento, desbordamiento interno y externo del desbordamiento de doble tubo de rebosadura hidrociclón fue realizado. Los resultados muestran que puede obtenerse tres diferentes clasificaciones en grado de producto, a saber, subdesbordamiento, desbordamiento interior y desbordamiento exterior. Los parámetros estructurales han demostrado que juegan un papel importante en la eficiencia de la clasificación del hidrociclon con doble vórtice finders. Este estudio proporciona una buena referencia para la optimización de los parámetros estructurales de doble tubo de rebosadura de los hidrociclones.
- **Palabras clave:** Ciclón, hidróciclon con doble vórtice finders, eficiencia de clasificación, parámetros estructurales, simulación numérica.

ABSTRACT

Classification efficiency of hydrocyclone is one of the kernel problems requiring solutions to promote the development of a solid–liquid separation system. A new hydrocyclone model was proposed to improve traditional structure and precise classification efficiency. Consequently, a coaxial overflow pipe with a small diameter was inserted into the original pipe, thereby possibly obtaining three different products with different size grades in one cycle. Then, using computational fluid dynamics, the Reynolds stress model was introduced into the Reynolds-averaged Navier–Stokes; the mathematical model of solid-liquid mixture multiphase flow was established. Finally, a study on the numerical simulation of the effects of structural parameters (e.g., underflow orifice diameter, internal overflow pipe diameter, and inserted depth of internal overflow pipe) on the classification efficiency of underflow, internal overflow, and external overflow of double overflow pipe hydrocyclones was conducted. Results show that one classification can obtain three different narrow-grade-classification products, namely, underflow, inner overflow, and outer overflow. The structural parameters are proven to play an important role in the classification efficiency of the hydrocyclone with double vortex finders. This study provides a good reference for the optimization of structural parameters of double overflow pipe hydrocyclones.

Keywords: Hydrocyclone with double vortex finders, Classification efficiency, Structural parameters, Numerical simulation.

1. INTRODUCTION

Hydrocyclones refer to devices that can separate phases with density difference or particle size difference using centrifugal sedimentation [1, 2]. Hydrocyclones have been widely used in the field of mineral processing, petroleum, chemical engineering, air pollution, power plants, and process industries because of the absence of its moving parts, simple structure, high working capacity, high separation efficiency, low maintenance costs, and small physical size of the device [3, 4]. Conventional single overflow pipe hydrocyclones can generate overflow and underflow only, resulting in broadly distributed size grades of the products. Notably, the classification efficiency of hydrocyclone is one of the kernel issues requiring solutions in the methods. A double overflow pipe hydrocyclone that can achieve precise grading is proposed to obtain several size grades in one cycle. More specifically, coaxial overflow pipes with different diameters are employed to expel fine particles from the internal overflow pipe; medium particles are expelled from the external overflow pipe, and coarse particles are expelled from the underflow orifice. Consequently, three different products with different size grades are obtained in one cycle. In contrast to conventional hydrocyclones focusing on hydrocyclone separation, the double overflow pipe hydrocyclone can achieve several products with a narrow particle size range, thus improving grading precision and reducing energy dissipation. Structural parameters, such as underflow orifice diameter, internal overflow pipe diameter, and inserted depth of internal overflow pipe, are important factors affecting hydrocyclone separation performance [5-10]. A reliable computer-aided design (such as computational fluid dy-

namics (CFD) package with fluid flow equations) is employed to analyze the effect of geometry changes and structural parameters on cyclone efficiency. Therefore, designing a new structural hydrocyclone is necessary to deal with the aforementioned problem.

The structure and size of the hydrocyclone are highly significant to the separation efficiency. Recently, the influence of different structures of the hydrocyclone on the separation efficiency has been investigated by many researchers at home and abroad. D.P. Obeng and S. Morrell et al. [11, 12] designed a hydrocyclone with two coaxial overflow tubes and with different diameters. Therefore, one classification can obtain three different narrow-grade-classification products, namely, the inner overflow, the outer overflow, and the underflow. The separation of two different density particles in a three-product hydrocyclone [13, 14] was investigated, and three different diameter particles were obtained. Mahmoud M. Ahmed et al. [6] designed a three-product hydrocyclone; the coarse particle was sent back to the ball mill, and the fine grinding rate of the ball grinding mill was improved. P. Bagdi et al. [15-20] investigated the grading efficiency of double overflow pipe hydrocyclones using numerical simulations. However, all the aforementioned studies did not consider the influence of structural parameters on the separation efficiency. Thus, improved work must be conducted to examine the influence of the underflow diameter, the overflow diameter, and the insertion depth of the overflow tube on separation ratio and classification efficiency. This study utilizes software FLUENT6.3 and the mixture multiphase flow model to establish the mathematical model of the solid-liquid multiphase flow for a hydrocyclone with a two-overflow-tube structure.

The remainder of this paper is organized as follows: Section 2 describes the methodology of the model of the cyclone separator with double vortex finders and the numerical method. Section 3 presents the numerical simulation results using CFD. The conclusions are summarized in Section 4.

2. MATERIALS AND METHODS

This model includes two main steps. The first step is establishing the mathematical model of the hydrocyclone with double vortex finders. This step introduces the Reynolds stress model into the Reynolds-averaged Navier–Stokes. Mixture models of gas–liquid and solid–liquid multiphase flows for a hydrocyclone with a two-overflow-tube structure are established. The second step is establishing the flow field model and boundary conditions. In this step, inlet conditions, flow rate, particle size, and volumetric concentrations of the feedstock are introduced and outlet conditions, wall modification, and numerical simulations are determined.

2.1. MATHEMATICAL MODEL OF THE HYDROCYCLONE

The structure of the hydrocyclone is cylindrical, and flow motion inside the hydrocyclone is rotational. Therefore, the equation of flow motion in the hydroyclone is described using a cylindrical coordinate system.

The continuity equation is expressed as follows:

$$\frac{1}{r}\frac{\partial u_\theta}{\partial \theta}+\frac{\partial u_r}{\partial r}+\frac{\partial u_z}{\partial z}+\frac{u_r}{r}=0 \tag{1}$$

N-S (Navier-Stokes) equation is expressed as follows:

$$\rho\left(u_r\frac{\partial u_r}{\partial r}+u_z\frac{\partial u_r}{\partial z}-\frac{u\theta^2}{r}\right)=-\frac{\partial \vec{P}}{\partial r}+\mu\left(\frac{\partial^2 u_r}{\partial r^2}+\frac{1}{r}\frac{\partial u_r}{\partial r}+\frac{\partial^2 u_r}{\partial z^2}-\frac{u_r}{r^2}\right) \tag{2}$$

$$\rho\left(u_r\frac{\partial u_\theta}{\partial r}+u_z\frac{\partial u_\theta}{\partial z}+\frac{u_r u_\theta}{r}\right)=\mu\left(\frac{\partial^2 u_\theta}{\partial r^2}+\frac{1}{r}\frac{u_\theta}{\partial r}+\frac{\partial^2 u_\theta}{\partial z^2}-\frac{u_\theta}{r^2}\right) \tag{3}$$

$$\rho\left(u_r\frac{\partial u_z}{\partial r}+u_z\frac{\partial u_z}{\partial z}\right)=-\frac{\partial \vec{P}}{\partial z}+\mu\left(\frac{\partial^2 u_z}{\partial r^2}+\frac{1}{r}\frac{u_z}{\partial r}+\frac{\partial^2 u_z}{\partial z^2}\right) \tag{4}$$

Concerning the nature of turbulence, Reynolds proposed the theory of time-averaged flow field, which divides the instantaneous motion parameters into two parts, namely, the time-averaged values and the fluctuating values.

$$u=\overline{u}+u' \tag{5}$$

Where, u, $\overline{u}$ and u' are instantaneous velocity, time-averaged velocity and fluctuating velocity, respectively. Substituting the equation (5) into the continuity equation and N-S equation, The continuity equation and the N-S equation in cylindrical coordinate system are expressed as follows:

$$\frac{1}{r}\frac{\partial u_\theta}{\partial \theta}+\frac{\partial u_r}{\partial r}+\frac{\partial u_z}{\partial z}+\frac{u_r}{r}=0 \tag{6}$$

$$\rho\left(u_r\frac{\partial u_r}{\partial r}+u_z\frac{\partial u_r}{\partial z}-\frac{u\theta^2}{r}\right)=-\frac{\partial \vec{P}}{\partial r}+\mu\left(\frac{\partial^2 u_r}{\partial r^2}+\frac{1}{r}\frac{\partial u_r}{\partial r}+\frac{\partial^2 u_r}{\partial z^2}-\frac{u_r}{r^2}\right) -\rho\left(\frac{1}{r}\frac{\partial}{\partial r}\overline{ru_r'^2}+\frac{\partial}{\partial z}\overline{u_r'u'}_z+\frac{1}{r}\overline{u_\theta'^2}\right) \tag{7}$$

$$\rho\left(u_r\frac{\partial u_\theta}{\partial r}+u_z\frac{\partial u_\theta}{\partial z}+\frac{u_r u_\theta}{r}\right)=\mu\left(\frac{\partial^2 u_\theta}{\partial r^2}+\frac{1}{r}\frac{u_\theta}{\partial r}+\frac{\partial^2 u_\theta}{\partial z^2}-\frac{u_\theta}{r^2}\right) -\rho\left(\frac{\partial}{\partial r}\overline{u_r'u'}_\theta+\frac{\partial}{\partial z}\overline{u_\theta'u'}_z+\frac{2}{r}\overline{u_r'u'}_\theta\right) \tag{8}$$

$$\rho\left(u_r\frac{\partial u_z}{\partial r}+u_z\frac{\partial u_z}{\partial z}\right)=-\frac{\partial \vec{P}}{\partial z}+\mu\left(\frac{\partial^2 u_z}{\partial r^2}+\frac{1}{r}\frac{u_z}{\partial r}+\frac{\partial^2 u_z}{\partial z^2}\right) -\rho\left(\frac{\partial}{\partial r}\overline{u_r'u'}_z+\frac{\partial}{\partial z}\overline{u_z'^2}\right) \tag{9}$$

2.2. FLOW FIELD MODEL AND BOUNDARY CONDITIONS

Fig. 1. shows the hydrocyclone with double vortex finders. This study proposes a three-product hydrocyclone with two overflow tubes. The hydrocyclone is designed with two coaxial overflow tubes with different diameters. During overflow, light and fine particles exit from the inner overflow tube. The mid-sized particles overflow from the outer overflow tube. The coarse particles can be obtained from the underflow tube. Therefore, one classification can obtain three different narrow-grade-classification products, namely, underflow, inner overflow, and outer overflow. Fig. 2. shows the flow field model of double overflow pipe hydrocyclones. Table I. shows the structural parameters. Using an structured mesh arrangement with hexahedral elements, the meshing results of the hydrocyclone were obtained as shown in Fig. 3. and there are 140577 nodes in total. The influences of mesh number and grid type on the simulation accuracy were analyzed. The results proved that the separation efficiency is independent of the mesh size and grid type.

The Reynolds stress model and mixture multiphase flow model were involved. Since the RSM (Reynolds Stress Model) accounts for the effects of streamline curvature, swirl, rotation, and rapid changes in strain rate, it has greater potential to give accurate predictions for simulating cyclone flows.

The mixture model is designed for two or more phases. The

mixture model solves for the mixture momentum equation and prescribes relative velocities to describe the dispersed phases.

The boundary conditions are defined as follows:

Inlet conditions: The flow rate is 5 m/s, $CaCO_3$ particles with seven different sizes (1, 5, 10, 15, 20, 30, and 40 μm) were introduced, and the volumetric concentration of the feedstock is 3.5% (0.3%, 0.5%, 0.7%, 0.7%, 0.5%, 0.5%, and 0.3% for different particles).

Outlet conditions: The overflow orifice and underflow orifice were pressure outlets.

Wall modification: No permeation or sliding were assumed to have been observed, and near wall modification using standard wall functions was involved to improve the calculation precision.

Fig. 1: Photo of the three-product hydrocyclone

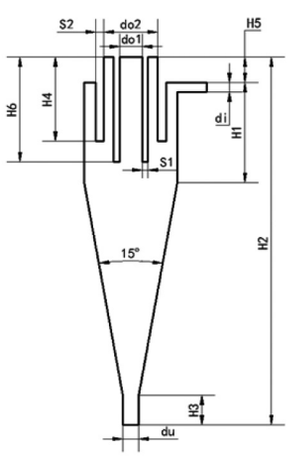

Fig. 2: Flow field of the cyclone

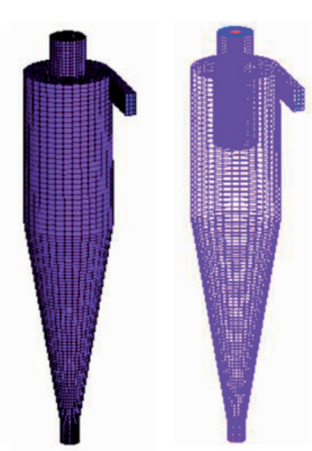

Fig. 3: Meshes of the hydrocyclone

In the numerical simulations, the pressure/speed coupling was treated using the SIMPLE pattern; the pressure dispersion of the governing equations was achieved using the PRESTO pattern; and the momentum dispersion was achieved using the QUICK pattern.

Structural parameter	Structural dimensions
Hydrocyclone diameter D (mm)	50
Inner vortex finder diameter d_{o1} (mm)	5, 6, 7, 9, 10
Outer vortex finder diameter d_{o2} (mm)	20
Underflow port diameter d_u (mm)	6, 8, 10, 12, 14
Feed inlet equivalent diameter d_i (mm)	12
Outer overflow pipe insertion depth H_4 (mm)	85
Inner overflow pipe insertion depth H_6 (mm)	65, 75, 85, 95, 105
Thickness of the overflow pipe s_1, s_2 (mm)	2, 2.5
Extension length of the overflow pipe H_5 (mm)	28
Cylinder height H_1 (mm)	116
Total height H_2 (mm)	310
Underflow pipe height H_3 (mm)	15

Table I:. Main structural parameters of the hydrocyclone with double vortex finders

3. RESULTS AND DISCUSSIONS

3.1. SIMULATION MODEL VERIFICATION

In the paper, with the same parameters, the simulation model verification of the hydrocyclone with the diameter of 75mm proposed by Hsieh is firstly carried out. The simulation results are compared with the measured data of the flow field studied by Hsieh [21] in 1988 with LDV (Laser Doppler Velocimetry), as shown in Fig. 4, which shows that the simulation results are basically consistent with the experimental data. Then the simulation model and the solution are reasonable, and the internal flow field of hydrocyclone can be predicted well by simulation.

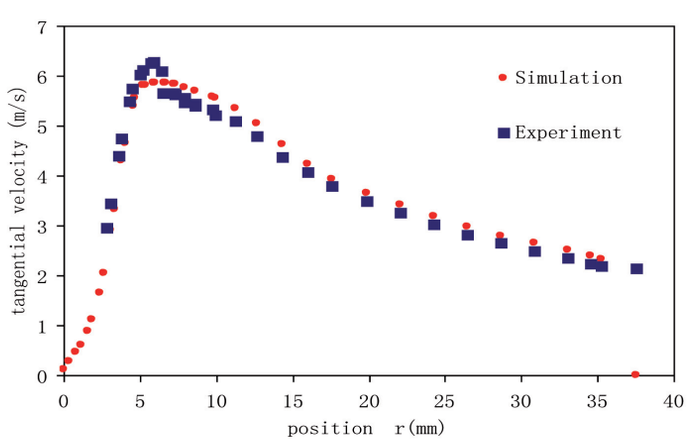

Fig. 4: Comparisons of tangential velocity between simulation and experiment

3.2. EFFECTS OF UNDERFLOW ORIFICE DIAMETER ON UNDERFLOW GRADING EFFICIENCY

The parameters of the hydrocyclones mentioned Table I used are as follows: diameter of external overflow pipe is 20 mm; diameter of internal overflow pipe diameter is 6 mm; and inserted depth of internal overflow pipe is 85 mm. Grading efficiency

curves of the double overflow pipe hydrocyclone in cases where the underflow orifice diameter is 6, 8, 10, 12, and 14 mm were obtained. Furthermore, the effects of underflow orifice diameter on underflow grading efficiency were investigated.

Particle separation efficiency at the underflow orifice refers to the mass flow rate ratio of the target particles and the feedstock particles after separation. The underflow orifice particle separation efficiency with particle sizes of 1, 5, 10, 15, 20, 30, and 40 μm and underflow orifice diameters of 6, 8, 10, 12, and 14 mm were obtained by simulatinng. The results showed that the particle separation efficiency at the underflow orifice increases (i.e., more coarse particles are separated) with the particle diameter. The separation size (d_{50}) is defined as the particle size corresponding to the underflow separation efficiency of 50%, indicating that the possibilities of these particles being expelled from underflow orifice and overflow orifice were 50%. For solid–liquid hydrocyclones, particles with diameters $<d_{50}$ are expelled from the overflow orifice, whereas particles with diameters $>d_{50}$ are expelled from the underflow orifice. d_{50} was 22, 19, 18, 14, and 8 μm for the underflow orifice diameters of 6, 8, 10, 12, and 14 mm, respectively. Considering that a small separation size indicates a high recovery rate of the hydrocyclone, the underflow orifice diameter should be increased to improve the hydrocyclone recovery rate.

The underflow productivity increased with the underflow orifice diameter, regardless of the particle size. However, the underflow productivity does not indicate the separation precision of the hydrocyclone. Indeed, the increase magnitudes of different particles were significantly different, as follows: the increase magnitudes of fine particles were larger than that of coarse particles. In other words, the particle size was reduced as the underflow orifice diameter increased. As coarse particles are preferred at the end of the separation, the underflow orifice diameter should be reduced.

3.3. EFFECTS OF INTERNAL OVERFLOW PIPE DIAMETER ON UNDERFLOW GRADING EFFICIENCY

The parameters of the double overflow pipe hydrocyclones used are as follows: the diameter of the external overflow pipe is 20 mm, the diameter of the underflow orifice diameter is 6 mm, and the inserted depth of the internal overflow pipe is 85 mm. The underflow grading efficiency curves of the double overflow pipe hydrocyclone in cases where the diameter of the internal overflow pipe is 5, 7, 9, and 10 mm were obtained.

The particle separation efficiency at the underflow orifice increases with the particle diameter. d_{50} is 22.5, 21, 19, and 17.5 μm for the internal overflow pipe diameters of 5, 7, 9, and 10 mm, respectively. As the separation size decreases as the internal overflow pipe diameter increases, the internal overflow pipe diameter should be increased to improve the hydrocyclone recovery rate.

The underflow productivity increased with the underflow orifice diameter, regardless of the particle size. However, the increase magnitudes of different particles were significantly different, as follows: the increase magnitudes of fine particles (<20 μm) were larger than that of coarse particles (30 or 40 μm). In other words, the particle size was reduced as the underflow orifice diameter increased. Therefore, the internal overflow pipe diameter should be reduced.

3.4. EFFECTS OF OVERFLOW PIPE INSERTED DEPTH ON THE UNDERLOW GRADING EFFICIENCY

The parameters of the double overflow pipe hydrocyclones used are as follows: the diameter of the external overflow pipe is 20 mm, the diameter of the internal overflow pipe diameter is 6 mm, the diameter of the underflow orifice diameter is 6 mm, and the inserted depth of the external overflow pipe is 85 mm. Grading efficiency curves of the double overflow pipe hydrocyclone in cases where the inserted depth of the internal overflow pipe is 65, 75, 85, 95, and 105 mm were obtained. The particle separation efficiency at the underflow orifice increases with the particle diameter. d_{50} is 20, 21, 22, 23, and 24 μm for the inserted depths of the internal overflow pipe of 65, 75, 85, 95, and 105 mm, respectively. d_{50} increased with the inserted depth of the internal overflow pipe, indicating that the inserted depth of the internal overflow pipe should be reduced.

Fig. 5. illustrates the underflow grading efficiency curves at different internal overflow pipe diameters and feedstock particles (X-axis is the inserted depth of internal overflow pipe and Y-axis is the underflow productivity). As shown in the figure, the underflow productivity decreased as the inserted depth of the internal overflow pipe increased, regardless of the particle size. This finding can be attributed to the axial flow rate, which decreases as the inserted depth of the internal overflow pipe increases. As the axial flow rate decreases, the residence duration of particles increases, which resulted in improved particle separation. Conversely, vertical moving distances of particles in the upstream are reduced, and increasing fine particles enter the overflow pipe. However, the decrease magnitudes of different particles were significantly different, as follows: the decrease magnitudes of fine particles (<15 μm) and coarse particles (>40 μm) were smaller than that of particles with diameters between 20 μm and 30 μm. This finding can be attributed to 20 and 30 μm, which are close to d50 in this case. Conversely, the distance from the internal overflow pipe and cone wall decreases, and the zero-velocity envelop panel shifts outward as the inserted depth increases. Consequently, several particles in the underflow join the overflow. Therefore, the effects of the inserted depth of the internal overflow pipe on the underflow particle diameter are dependent on the decrease magnitudes of underflow productivity corresponding to different particle sizes as follows: underflow particle size decreases as the decrease magnitude of underflow productivity increases and vice versa.

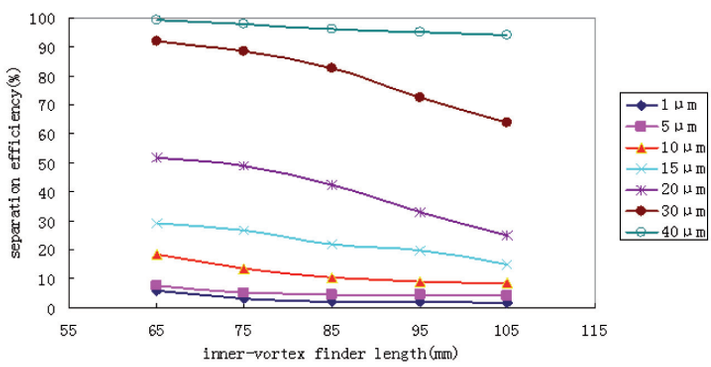

Fig. 5: Effect of the inner vortex finder length on the separation efficiency

3.5. EFFECTS OF UNDERFLOW ORIFICE DIAMETER ON THE RECOVERY RATE OF INTERNAL OVERFLOW PARTICLES

The recovery rate of internal overflow particles is defined as the mass flow rate ratio of the target particles at the internal overflow orifice and the feedstock particles after separation. The underflow orifice particle separation efficiency with particle sizes of 1, 5, 10, 15, 20, 30, and 40 μm and the underflow orifice diameter is 6, 8, 10, 12, and 14 mm were obtained through numerical simulations. Obviously, the recovery rate of internal overflow

particles decreased as the particle size increased, and the content of fine particles was significantly higher than that of coarse particles. Furthermore, the internal overflow productivity was negligible at an underflow orifice diameter of 12 or 14 mm. This finding can be attributed to the internal overflow pipe being occupied by air columns, and no particles can be expelled from the internal overflow pipe.

Fig. 6. illustrates the recovery rates of the internal overflow particles at different underflow orifice diameters (X-axis is the underflow orifice diameter and Y-axis is the internal overflow productivity). As shown in the figure, the recovery rate of the internal overflow particles decreased significantly as the underflow orifice diameter increased, and the decrease magnitude increased as the particle size decreased. In other words, the content of fine particles exhibited a larger decrease magnitude, indicating that the recovery rate of the internal overflow particles decreases and the particle size increases as the underflow orifice diameter increases.

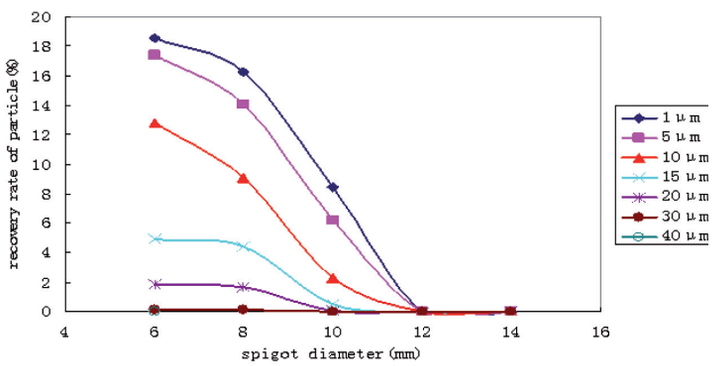

Fig. 6: Effect of the spigot diameter on the inner vortex recovery rate

3.6. EFFECTS OF OVERFLOW PIPE DIAMETER ON THE RECOVERY RATE OF THE INTERNAL OVERFLOW PARTICLES

The recovery rates of the internal overflow particles with seven different sizes (1, 5, 10, 15, 20, 30, and 40 μm) in cases where the diameter of the internal overflow pipe is 5, 7, 9, and 10 mm were obtained through numerical simulations. The content of particles in the internal overflow decreases as the particle size increases. At the internal overflow pipe diameter of 5 mm, the internal overflow pipe was occupied by air columns, and no particles can be recovered from the internal overflow pipe.

Fig. 7. illustrates the recovery rates of the internal overflow particles at different internal overflow pipe diameters (X-axis is the internal overflow pipe diameter and Y-axis is the internal overflow productivity). As shown in the figure, the recovery rate of internal overflow particles increases with the internal overflow pipe diameter. Furthermore, the increase magnitudes of fine particles were larger than that of coarse particles, indicating that the size of internal overflow particles decreases as the internal overflow pipe diameter increases.

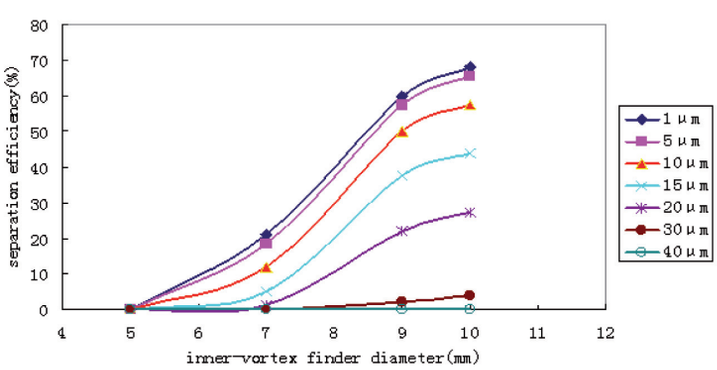

Fig. 7: Effect of the inner vortex finder diameter on the inner vortex recovery rate

3.7. EFFECTS OF OVERFLOW PIPE INSETED DEPTH ON THE RECOVERY RATE OF INTERAL OVERFLOW PARTICLES

The recovery rates of internal overflow particles with seven different sizes (1, 5, 10, 15, 20, 30, and 40 μm) were obtained through numerical simulations in cases where the inserted depth of the internal overflow pipe is 65, 75, 85, 95, and 105 mm. The recovery rate decreases as the particle size increases, indicating that the content of fine particles in the internal overflow was relatively high. Furthermore, the recovery rate of internal overflow particles was affected by the inserted depth of internal overflow pipe. At the inserted depth of the internal overflow pipe of 85 mm (same as the inserted depth of the external overflow pipe), the recovery rate was maximized.

Fig. 8. illustrates the recovery rates of internal overflow particles at different inserted depths of the internal overflow pipe (X-axis is the inserted depth of the internal overflow pipe and Y-axis is the internal overflow productivity). In cases where the inserted depth of the internal overflow pipe is less than the inserted depth of the external overflow pipe, the recovery rate of internal overflow particles increases with the inserted depth of the internal overflow pipe. Moreover, the increase magnitude of fine particles was larger than that of coarse particles, indicating that the size of particles in the internal overflow decreased. In cases where the inserted depth of the internal overflow pipe is greater than the inserted depth of the external overflow pipe, the recovery rate of internal overflow particles decreases with the inserted depth of the internal overflow pipe.

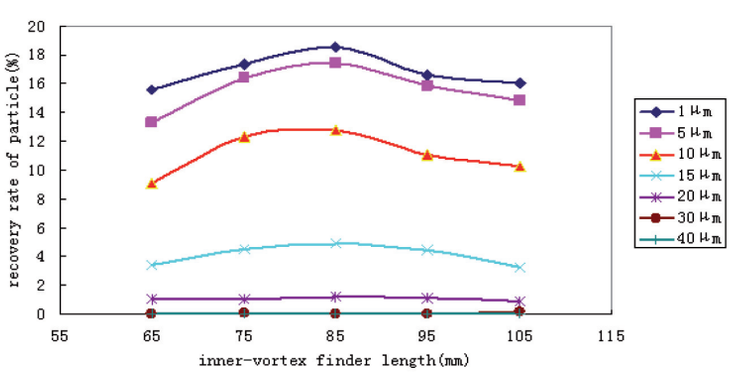

Fig. 8: Effect of the inner vortex finder length on the inner vortex recovery rate

3.8. EFFECTS OF UNDERFLOW ORIFICE DIAMETER ON THE RECOVERY RATE OF EXTERNAL OVERFLOW PARTICLES

The recovery rate of external overflow particles is defined as the mass flow rate ratio of the target particles at the external overflow orifice and the feedstock particles after separation. The recovery rates of external overflow particles with seven different sizes (1, 5, 10, 15, 20, 30, and 40 μm) were obtained through numerical simulations in cases where the underflow orifice diameter is 6, 8, 10, 12, and 14 mm. The content of fine particles was significantly higher than that of coarse particles. Furthermore, the decrease magnitude of coarse particles in the external overflow resulting from an increasing particle size was lower than that of coarse particles in the underflow, whereas the content of coarse particles in the internal overflow decreased rapidly as the particle

size increased. In other words, the size of particles in the external overflow was larger than that of the particles in the internal overflow.

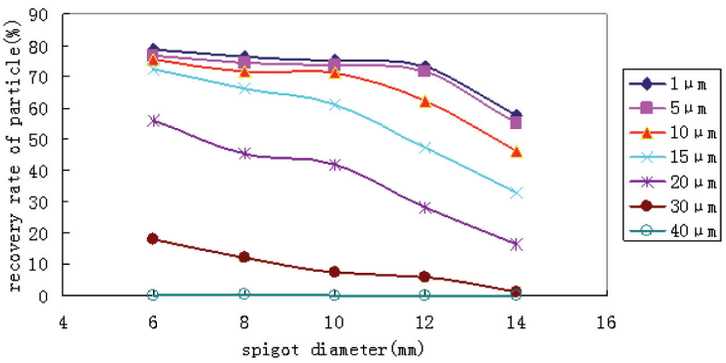

Fig. 9: Effect of the spigot diameter on the outer vortex recovery rate

Fig. 9. illustrates the recovery rates of external overflow particles at different underflow orifice diameters (X-axis is the underflow orifice diameter and Y-axis is the external overflow productivity). As shown in the figure, the recovery rate of external overflow particles increases with the underflow orifice diameter. Given the decreasing content of coarse particles, the size of particles in the external overflow decreases as the underflow orifice diameter increases.

3.9. EFFECTS OF INTERNAL OVERFLOW PIPE DIAMETER ON THE RECOVERY RATE OF EXTERNAL OVERFLOW PARTICLES

Fig. 10. shows the recovery rate curves of external overflow particles with particle size of 1, 5, 10, 15, 20, 30, and 40 μm and internal overflow pipe diameter of 5, 7, 9, and 10 mm. Obviously, the recovery rate of external overflow particles in double overflow pipe hydrocyclones decreases as the particle size increases. Fig. 11. illustrates the effects of internal overflow pipe diameter on the recovery rate of external overflow particles. Compared with the recovery rate of coarse particles, the recovery rate of fine particles decreases more significantly with the internal overflow pipe diameter. Combined with simulation analysis, the size of particles in the external overflow can be concluded to increase with the diameter of the internal overflow pipe.

3.10. EFFECTS OF THE INSERTED DEPTH OF THE INTERAL OVERFLOW PIPE ON THE RECOVERY RATE OF EXTERNAL OVERFLOW PARTICLES

Fig. 12. shows the recovery rate curves of external overflow particles with inserted depth of the internal overflow pipe of 65, 75, 85, 95, and 105 mm, and the particle size is 1, 5, 10, 15, 20, 30, and 40 μm, respectively.

As shown in Fig. 12. The content of fine particles in the external overflow was higher than that of coarse particles. In cases where the inserted depth of the internal overflow pipe is <85 mm, the contents of coarse particles (d = 30 μm) and fine particles (d = 10, 15, and 20 μm) increase with the inserted depth; whereas the content of fine particles increases more rapidly. In cases where the inserted depth of the internal overflow pipe is larger than the inserted depth of the external overflow pipe, the content of fine particles increases at a significantly higher rate with the inserted depth of the internal overflow pipe, indicating that the size of

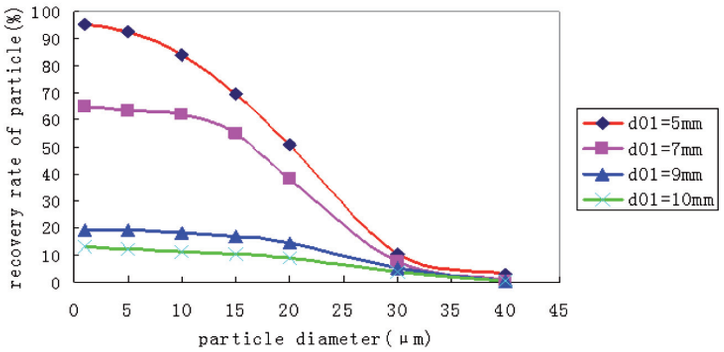

Fig. 10: Effect of the particle diameter on the outer vortex recovery rate

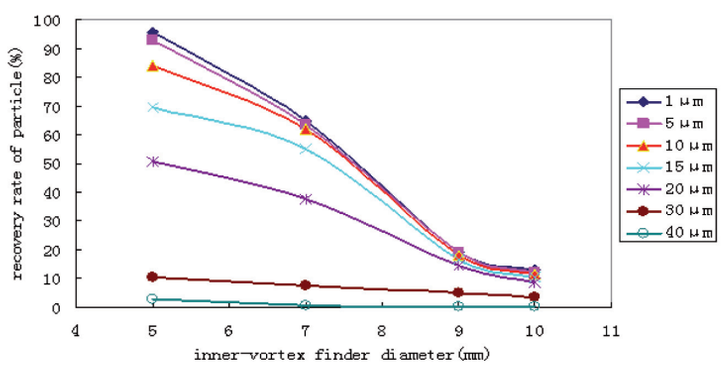

Fig. 11: Effect of the inner vortex finder diameter on the outer vortex recovery rate

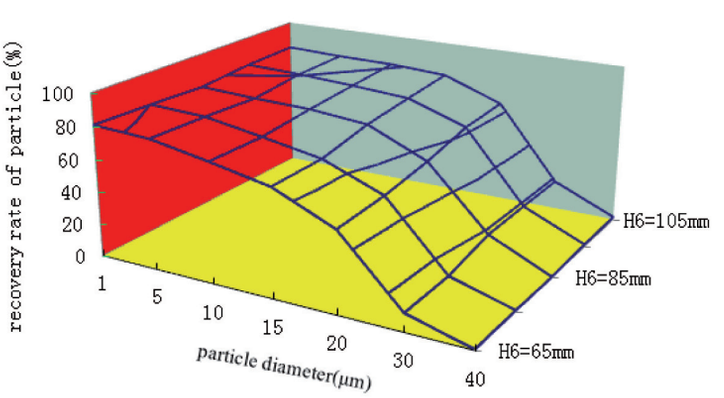

Fig. 12: Effect of the particle diameter on the outer vortex recovery rate

particles in the external overflow decreases as the inserted depth of the internal overflow pipe increases.

4. CONCLUSIONS

In this study, a precise grading double overflow pipe hydrocyclone that can achieve three different products with different size grades in one cycle is proposed. Using CFD, the influence of the underflow diameter, the overflow diameter, and the insertion depth of the overflow tube on classification efficiency is obtained. The results show that structural parameters play an important role in classification efficiency.

(1) The underflow productivity increases as the underflow orifice diameter increases, the diameter of the internal overflow pipe increases, and the inserted depth of the internal overflow pipe decreases.

(2) The numerical simulations revealed that the size of underflow particles decreased as the underflow orifice diameter increased and the diameter of the internal overflow pipe increased. The effects of the inserted depth of the internal overflow pipe on the size of underflow particles are dependent on the initial contents and decrease magnitudes of different particles.

(3) The size of the internal overflow particles increases and the internal overflow productivity decreases as the underflow orifice diameter increases. The effect of the inserted depth of the internal overflow pipe on the internal overflow productivity is negligible.

(4) The effects of the underflow orifice diameter, the diameter of the internal overflow pipe, and the inserted depth of the internal overflow pipe on the recovery rate of external overflow particles are as follows: the recovery rate and size of external overflow particles decrease as the underflow orifice diameter increases; the recovery rate of the external overflow particles decreases, whereas their size increases as the diameter of internal overflow pipe increases; the size of the external overflow particles decreases with the inserted depth of the internal overflow pipe, although its effect on the recovery rate of external overflow particles is negligible.

The results obtained in the study have important theoretical and practical values in engineering and will be valuable to explain the separation essence fully, explore the separation principle, enrich rotational flow classification theory, and develop energy-efficient multiproduct hydrocyclones. Further research based on this model is required, particularly for the cone angle and feeding inlet of a three-product hydrocyclone.

BIBLIOGRAPHY

[1] Bhasker C. "Flow simulation in industrial cyclone separator". Advances in Engineering Software. February 2010. Vol.41-2. p. 220-228. DOI: http://dx.doi.org/10.1016/j.advengsoft.2009.08.004.

[2] Pei-Kun Liu, Liang-Yin Chu, Jing Wang, et al. "Enhancement of Hydrocyclone Classification Efficiency for Fine Particles by Introducing a Volute Chamber with a Pre-Sedimentation Function". Chemical Engineering and Technology. March 2008. Vol.31. p. 474-478. DOI: http://dx.doi.org/10.1002/ceat.200700449.

[3] Z. Qi,S.B. Kuang, A.B. Yu. "Numerical investigation of the separation behaviours of fine particles in large dense medium cyclones". International Journal of Mineral Processing. September 2015. Vol.142. p.35–45. DOI: http://dx.doi.org/10.1016/j.minpro.2015.05.006.

[4] Dwari R.K., Biswas M.N., Meikap B.C. "Performance characteristics for particles of sand FCC and fly ash in a novel hydrocyclone". Chemical Engineering Science. February 2004. Vol. 59. p.671–684. DOI: http://dx.doi.org/10.1016/j.ces.2003.11.015.

[5] Mainza A., Narasimha M. Powell M.S. et al. "Study of flow behaviour in a three-product cyclone using computational fluid dynamics". Minerals Engineering. August 2006. Vol.19. p. 1048-1058. DOI: http://dx.doi.org/10.1016/j.mineng.2006.03.014.

[6] Mahmoud M. Ahmed, Galal A. Ibrahim, Mohamed G. Farghaly. "Performance of a three-product hydrocyclone". International Journal of Mineral Processing. April 2009.Vol.91.p. 34-40. DOI: http://dx.doi.org/10.1016/j.minpro.2008.11.005.

[7] M. Ghodrat, S.B. Kuanga, A.B. Yua, et al. "Numerical analysis of hydrocyclones with different vortex finder configurations". Minerals Engineering. August 2014. Vol 63. p.125–138. DOI: http://dx.doi.org/10.1016/j.mineng.2014.02.003.

[8] Narasimha M., Mainza A.N., Holtham P.N. "A semi-mechanistic model of hydrocyclones - Developed from industrial data and inputs from CFD". International Journal of Mineral Processing. December 2014. Vol.133. p.1-12. DOI: http://dx.doi.org/10.1016/j.minpro.2014.08.006.

[9] M. Ghodrat, S. B. Kuang, A. B. Yu, et al. "Computational Study of the Multiphase Flow and Performance of Hydrocyclones: Effects of Cyclone Size and Spigot Diameter". Industrial and Engineering Chemistry Research. November 2013. Vol.52. p.16019-16031. DOI: http://dx.doi.org/10.1021/ie402267b.

[10] Y. Rama Murthy, K. Udaya Bhaskar. "Parametric CFD studies on hydrocyclone". Powder Technology. November 2012 Vol. 230.p.36-47.DOI: http://dx.doi.org/10.1016/j.powtec.2012.06.048.

[11] D.P. Obeng, S. Morrell. "The JK three-product cyclone-performance and potential applications". International Journal of Mineral Processing. March 2003.Vol.69. p. 129-142. DOI: http://dx.doi.org/10.1016/S0301-7516(02)00125-4.

[12] D.P. Obeng, S. Morrell, T.J. Napier-Munn. "Application of central composite rotatable design to modelling the effect of some operating variables on the performance of the three-product cyclone". International Journal of Mineral Processing. June 2005. Vol.76. p. 181-192. DOI: http://dx.doi.org/10.1016/j.minpro.2005.01.002.

[13] Mainza A., Powell M.S., Knopjes B. "Differential classification of dense material in a three-product cyclone". Minerals Engineering. June 2004. Vol.17. p.573-579. DOI: http://dx.doi.org/10.1016/j.mineng.2004.01.023.

[14] Ahmed, Mahmoud M., Ibrahim, Galal A.,Farghaly, Mohamed G. "Performance of a three-product hydrocyclone". International Journal of Mineral Processing. April 2009. Vol.91. p.34-40. DOI: http://dx.doi.org/10.1016/j.minpro.2008.11.005.

[15] P. Bagdi, P. Bhardwaj, A. K. Sen. "Analysis and Simulation of a Micro Hydrocyclone Device for Particle Liquid Separation". Journal of Fluids Engineering. 2012. Vol.134. p. 1-9. DOI: http://dx.doi.org/10.1115/1.4006020.

[16] Yanxia Xu, Xingfu Song, Ze Sun et al. Numerical Investigation of the Effect of the Ratio of the Vortex-Finder Diameter to the Spigot Diameter on the Steady State of the Air Core in a Hydrocyclone. "Industrial and Engineering Chemistry Research". April 2013. Vol.52. p.5470-5478. DOI: http://dx.doi.org/10.1021/ie302081v.

[17] Sonali Swain, Swati Mohanty. "A 3-dimensional Eulerian–Eulerian CFD simulation of a hydrocyclone". Applied Mathematical Modelling. March 2013, Vol.37. p. 2921–2932. DOI: http://dx.doi.org/10.1016/j.apm.2012.06.007.

[18] Y.Rama Murthy, K.Udaya Bhaskar. "Parametric CFD studies on hydrocyclone". Powder Technology. November 2012. Vol.230. p.36–47. DOI: http://dx.doi.org/10.1016/j.powtec.2012.06.048.

[19] S.B. Kuang, K.W. Chu, A.B. Yu, et al. "Numerical study of liquid-gas-solid flow in classifying hydrocyclones: effect of feed so1ids concentration". Minerals Engineering. May 2012. Vol.31. p.17–31. DOI: http://dx.doi.org/10.1016/j.mineng.2012.01.003.

[20] Cullivan J.C., Williams R.A., Cross C.R. "Understanding the hydrocyclone separator through computational fluid dynamics". Chemical Engineering Research and Design. April 2003. Vol.81. p.455-466. DOI: http://dx.doi.org/10.1205/026387603765173718.

[21] Hsieh K T. A phenomenological model of the hydrocyclone [D]. Salt Lake City: University of Utah, 1988.

ACKNOWLEDGEMENTS

This study was supported by the National Natural Science Foundation of China (No.21276145) and Natural Science Foundation of Shandong province (ZR2013EEM016).